
EVALUATION OF FORCE FIELDS FOR MOLECULAR DYNAMICS SIMULATIONS OF PLATINUM IN BULK AND NANOPARTICLE FORMS

PUBLISHED IN: *J. Chem. Theory Comput.* 2021, 17, 7, 4486–4498

Ingrid M. Padilla Espinosa
Department of Mechanical Engineering
University of California, Merced
Merced, CA 95340, USA
ipadillaespinosa@ucmerced.edu

Tevis D.B. Jacobs
Department of Mechanical Engineering and Materials Science
University of Pittsburgh
Pittsburgh, PA 15261, USA
tjacobs@pitt.edu

Ashlie Martini
Department of Mechanical Engineering
University of California, Merced
Merced, CA 95340, USA
amartini@ucmerced.edu

ABSTRACT

Understanding the size- and shape-dependent properties of platinum nanoparticles is critical for enabling design of nanoparticle-based applications with optimal and potentially tunable functionality. Towards this goal, we evaluated nine different empirical potentials with the purpose of accurately modeling faceted platinum nanoparticles using molecular dynamics simulation. First, the potentials were evaluated by computing bulk and surface properties – surface energy, lattice constant, stiffness constants, and the equation of state – and comparing these to experimental measurements and quantum mechanics calculations. Then, the potentials were assessed in terms of the stability of cubic and icosahedral nanoparticles with faces in the $\{100\}$ and $\{111\}$ planes, respectively. Although none of the force fields predicts all the evaluated properties with perfect accuracy, one potential – the embedded atom method formalism with a specific parameter set – was identified as best able to model platinum in both bulk and nanoparticle forms.

1 Introduction

The catalytic, electronic, optical, and thermal properties of platinum nanoparticles make them valuable materials for the pharmaceutical and specialty chemistry industries, [83, 5] for fuel cells, [38, 87, 54] and solar energy conversion, [11, 14] as well as for biomedical applications, [10] among others. However, platinum is an expensive transition metal and its reserves are limited. Therefore, studies have focused on improving platinum nanoparticle properties in an effort to reduce the amount of platinum required and decrease the associated costs. [98, 42]

Studies on catalysis have demonstrated that the efficiency of platinum nanoparticles increases as the particle size decreases [76] as a result of the increased surface-to-volume ratio. [105] When the size of the particle is reduced to just a few nanometers, the nanoparticles form facets and remain stable in shapes such as icosahedra, [77, 100] tetrahedra, [66, 22] cuboctahedra or “quasi spherical”, [1, 66, 85] cubes, [85, 66, 22, 41] and truncated octahedra, [60, 1, 85] These different nanoparticle shapes have different surface facets (mostly $\{111\}$, $\{110\}$, and $\{100\}$ [67, 85]) and different numbers of atoms at corners and edges that affect their overall properties. [16, 105] Since nanoparticle properties are dependent on shape and size, [78] it is desirable to understand and predict the evolution of their shape- and size-dependent properties throughout the service life of a given application.

Due to their small size, a comprehensive understanding of the shape- and size-dependence of nanoparticle properties is difficult to achieve experimentally. For example, the dependence of strength and deformation on particle size and shape has been investigated. Studies on the deformation of faceted gold nanoparticles using an anvil cell [73] have shown the occurrence of Shockley dislocations along facet vertices. However, to prevent sintering, the maximum load achieved with this method is limited, and the stress cannot be calculated directly, instead it is inferred from lattice changes. Separate *in situ* studies on the compression of silicon [31] and gold [18] nanoparticles using transmission electronic microscopy (TEM)–atomic force microscopy (AFM) have characterized reversible and irreversible deformation, as well as hardening–deformation relationships. But, these experiments are limited by AFM tip tilting, slip off of the nanoparticle from the tip, and lack of controllable strain rate. Additionally, the strain distribution caused by the substrate support in platinum nanoparticles has been studied with a scanning transmission electron microscope (STEM) [27] and has shown that the nanoparticles experience larger strain if the substrate is SnO₂ compared to C, affecting the electrochemical activity. [97] However, image resolution was adversely affected by the fast scans required to prevent beam damage and due to contamination from outgassing. For platinum nanoparticles, structural changes and strain during catalytic reactions have been observed using Bragg coherent diffraction imaging. [23] However, these measurements are sensitive to fluctuations in the scans from temperature differences between the nanoparticles and the media. All of these examples demonstrate the significant challenges to using experimental approaches to link the material properties and behavior of nanoparticles.

An alternative to experimental methods is simulation. The stability of clusters and very small nanoparticles, including platinum nanoparticles, has been studied previously [44, 101, 21, 65, 99] using density functional theory (DFT). Such DFT calculations can predict interatomic distances, cohesive energy, and binding energy with high accuracy, as well as the shape-stability and surface reconstruction of nanoparticles. However, DFT is severely limited in the number of atoms, and therefore nanoparticle size, that can be modeled. [95] The size scale of DFT also precludes investigation of the effects of strain due to substrate interactions or stress due to external loading on nanoparticle properties. Therefore, such calculations are usually limited to bulk materials or small clusters of atoms, and are difficult to apply to nanoparticles larger than few nanometers.

Instead, molecular dynamics (MD) simulations offer a valuable tool to study the shape- and size-dependence of small faceted metallic nanoparticles properties at scales large enough to be relevant to applications. Although molecular dynamics simulations do not account explicitly for molecular orbitals and so cannot reproduce electronic effects, [80] they provide reasonable accuracy for modeling fundamental microstructural mechanisms in equilibrium or for a deformed structure, the equation of state of a system, phase equilibrium, transport properties, etc. [86] In MD, the selection of potential, or force field, is fundamental for accurate characterization and prediction. [45, 46] Force fields can be categorized as pair potentials or many-body potentials. While pair potentials are simpler to implement, they have drawbacks for platinum and other FCC metals, often requiring the inclusion of volume dependent correction factors to properly match experimental data. [7] Also, pair potentials incorrectly estimate the relative magnitudes of vacancy formation and cohesive energies, resulting in incorrect stacking fault energies, surface structure, and relaxation properties. [24] In general, many-body potentials describe metallic systems more accurately than pair potentials and are able to capture the Cauchy discrepancy of elastic constants. [24]

Multiple different formalisms for many-body potentials exist. For metals, the embedded atom method (EAM), [40, 28] and other potentials based on it, such as Finnis–Sinclair, [37] concentration-dependent EAM, [17] and modified EAM (MEAM), [6] are widely used. Another many-body potential is the effective medium theory (EMT) for bonding in metallic systems, [51] which uses a simple form of the effective medium theory of condensed matter to define the potential energy. Additionally, sets of parameters for metallic systems are based on bond-order potentials extended from the Tersoff formulation, [91] such as the Brenner potential [9] and the charge optimized many body (COMB) potential. [81] Metallic systems have also been modeled using reactive force field (ReaxFF) [12] which is based on bond-orders. ReaxFF accounts for dynamic partial charge equilibrations in the system and captures chemical reactions. ReaxFF parameters have been developed for chemical systems of platinum interacting with carbon [35] and oxygen. [79] While parameters sets for all these potential formalisms have been developed for platinum, their relative accuracy, particularly for nanoparticles, has not been characterized.

Here, we evaluated nine different readily available and easily implementable potentials based on their ability to predict bulk and surface material properties: lattice constant, stiffness constants, equations of state, and surface energies of {100}, {110}, {111} facets. Model predictions were compared to previously reported experimental data and quantum mechanics calculations. Then, the potentials were further evaluated in terms of their ability to model the stability of platinum nanoparticles. Analysis of the calculated bulk and surface properties, as well as nanoparticle stability, show that, although none of the force fields can accurately model all properties, one of the potentials was identified as best able to model platinum in both bulk and nanoparticle forms. Our results provide the basis for selection of a force field to model platinum and platinum nanoparticles properties and behavior in future studies.

2 Methods

The nine different potentials for platinum evaluated in this study are listed in Table 1. Each potential is designated by the force field type in all capital letters hyphenated with the year that it was reported, as shown in the right most column of Table 1.

Ref.	Year	Force Field Type	Designation
39	1987	EAM	EAM-(1987) [*]
108	2004	EAM	EAM-(2004) [*]
6	1992	MEAM	MEAM-(1992)
59	2003	MEAM	MEAM-(2003) [*]
79	2008	ReaxFF	REAX-(2008)
35	2014	ReaxFF	REAX-(2014)
52	1996	EMT	EMT-(1996) ^ζ
2	2002	Tersoff-Brenner	TERSOFF-(2002) ^ζ
4	2017	COMB	COMB-(2017)

Table 1: Force fields evaluated in this work, organized by force field type.

EAM: Embedded atom method, MEAM: modified embedded atom method, COMB: Charge optimized many body, EMT: Effective medium theory. The superscript ^{*} indicates force field parameters obtained from the NIST repository [45] and ^ζ indicates parameters obtained from the openKIM project. [90]

Other force field formulations have been proposed for platinum [104, 13, 61, 70, 72, 24, 29, 71, 26, 53] and machine learning has been used recently to generate sets of force field parameters. [48, 19] However, here we considered only readily available and easily implementable force fields and parameters.

These force fields differ both in functional form as well as how they were parameterized, i.e., with what data the potential parameters were fit. The EAM and EAM-based force fields are robust potentials with only modest demands for computational resources and their formulation is particularly well suited to model pure metals and alloys. EAM is empirically fit to the sublimation energy, equilibrium lattice constants, elastic constants, and vacancy and interstitial formation energies. EAM potentials have been shown to reproduce surface reconstructions observed experimentally. [39] The EMT potential, like EAM, is well suited for metallic systems involving pure metals and metal alloys. By using the simplest medium description for the interatomic interactions, calculations with this force field are computationally inexpensive. The EMT potential was fit to cohesive energies, lattice constants, and bulk and shear moduli. The Tersoff-like potentials have been successful describing a wide range of materials, including covalently bonded and metallic systems. The set of parameters of TERSOFF-(2002) was fit for a metallic-covalent system Pt-C, and is capable predicting the structural and cohesive properties for both elements (Pt and C) individually in different crystal phases, as well as the interatomic interactions between the elements. The COMB-(2017) was fit to defect formation energies, surface energies and stacking fault energies, and its parameterization particularly focused on platinum nanoparticles. The REAX-(2014) parameters were fit to describe Pt-O interactions, oxygen adsorption, and oxide formation. These interactions are particularly valuable to study catalytic processes. The parameterization of bulk platinum was fit to the following bulk phases of platinum: face centered cubic; ideal hexagonal close-packed; body centered cubic; simple cubic; diamond cubic; and b-tungsten. The REAX-(2008) was focused on the parameters for platinum nanoclusters interacting with carbon platelets and hydrogen for electrocatalysis studies. One of the advantages of COMB and ReaxFF potentials is the possibility of coupling the single element parameters with different multi-component systems as well as the ability to capture the formation and breaking of chemical bonds. However, these potentials tend to be computationally more expensive due to the recalculation of partial charges, the determination of bond-orders, and because a very small time steps (0.1 fs - 0.25 fs) is required to properly capture the dynamics of the system.

As described in the prior paragraph, all of these potentials have been designed and fit to the properties of platinum; however, this fitting was primarily done for bulk systems. Therefore the open research question is how accurately do these various potentials describe the behavior of platinum nanoparticles, and which potential is most accurate. To answer this question, the potentials described in Table 1 were evaluated by calculating the lattice constant, surface energies, and stiffness constants, and modeling of the equation of state of bulk platinum; then these results were compared to previously reported experimental properties and density functional theory (DFT) calculations. Finally, the force fields

were used to model a cubic nanoparticle with faces in $\{100\}$ planes and an icosahedron with faces in $\{111\}$ planes at room temperature to compare the accuracy of predictions of nanoparticle stability.

All simulations were performed using the large scale atomic/molecular massively parallel simulator (LAMMPS) package. [75] For the dynamics simulations, the time step for ReaxFF and COMB force fields was 0.2 fs, and a time step of 1 fs was used for all the other force fields. The temperature of the dynamics simulations was controlled using a Nosé-Hoover thermostat with a damping parameter of 0.1 ps. And the pressure was controlled using a Nosé-Hoover barostat with a damping parameter of 1 ps.

For simulations of bulk and surface properties, two system sizes with approximately 16,000 and 19,000 atoms were modeled to evaluate possible size effects. The models were FCC single-crystal structures, created with the LAMMPS software. For all force fields, the maximum difference between the surface energies, stiffness constants, and bulk modulus calculated using the two different-size models was less than 0.09%. This minimal difference showed that the smaller system was large enough and was used subsequently for all bulk and surface property simulations.

2.1 Lattice Constant

The lattice parameter of "bulk" platinum was calculated by generating supercells based on the experimental lattice parameter for FCC platinum 0.392 nm. [56] Periodic boundary conditions were applied in all directions. The geometry was minimized using the conjugate gradient method while allowing the simulation box to relax in all directions to account for possible differences between the experimental lattice parameter and the lattice predicted by the force field. The temperature of the system was increased to 298 K and equilibrated for 100 ps using a canonical ensemble. This was followed by an isobaric-isothermal equilibration at 298 K and atmospheric pressure for an additional 100 ps, to allow changes in the dimensions of the systems. The force field-predicted lattice constant was calculated from the last 20 ps of the equilibrated structure of the isobaric-isothermal equilibration step.

2.2 Surface Energies

Small nanoparticles of varying shapes can form facets in different orientations and therefore different surface energies determine their catalytic, electronic, optical, and thermal properties. [69] Therefore, the ability of the potentials to predict the surface energy in different (hkl) faces was evaluated. In particular we calculated the surface energies for the (111), (110), and (100) planes. Most of the common nanoparticle geometries form facets oriented in the families of these planes. Also, the availability of DFT data for these surfaces in the literature enabled direct comparison.

A typical "slab" model as described below was used to calculate the surface energy of platinum. First, the atomic energy in "bulk" platinum was calculated by generating supercells as in the lattice parameter calculations. The geometry was minimized using the conjugate gradient method and the temperature of the system was increased to 298 K and equilibrated for 100 ps using a canonical ensemble. The increase in temperature introduces a small disturbance of the energy of the system to avoid energetic local minima. After the equilibration process, the energy of the system was minimized again until the difference in energy between iterations divided by average energy was less than 1×10^{-12} . To simulate free surfaces, the supercells were oriented such that the (hkl) planes of the relevant surface were perpendicular to the x direction. A schematic of the orientation of the faces in the slab model can be seen in the Supporting Information. Vacuum layers of 5 nm in the x direction were constructed to provide exposed surfaces in both sides of the slab. Periodic boundary conditions were imposed in all directions. Then, the same MD simulation steps and settings as described for the "bulk" systems were followed, with the difference that the length of the simulation box was kept fixed in the x direction to preserve the free surface. The surface energy γ of a facet with Miller index (hkl) was calculated with the eq 1 [92]

$$\gamma_{hkl} = \frac{E_{slab} - E_{bulk/atom} \cdot N_{slab}}{2A_{slab}} \quad (1)$$

where E_{slab} is the total energy of the slab, $E_{bulk/atom}$ is the energy per atom of the oriented bulk system, N_{slab} is the number of atoms in the slab, and A_{slab} is the exposed surface area of the slab in one direction, assuming that the area remains constant at both exposed surfaces.

2.3 Stiffness Constants

A direct static method was used to statistically calculate elastic properties. In this analysis, the platinum supercell was relaxed using an energy minimization coupled with box adjustments towards zero pressure. Twelve infinitesimal deformations were introduced by changing the dimensions of the simulation box. These deformations correspond to six tensile and six pure shear strains of magnitude $\pm 5 \times 10^{-6}$. The system energy was minimized following each deformation. For infinitesimal strain, the stress-strain relationship can be assumed to be linear, so the stiffness constants

were calculated according to Hooke's law shown in eq 2.

$$\sigma_{ij} = C_{ijkl}\varepsilon_{kl} \quad (2)$$

where σ_{ij} is the stress tensor calculated from the Virial stress definition, [107] C_{ijkl} are the stiffness constants, and ε_{kl} is the strain imposed to the system in each direction. Two additional magnitudes of strain ($\pm 1 \times 10^{-6}$ and $\pm 5 \times 10^{-5}$) were tested and negligible difference (less than 0.01%) between the stiffness constants calculated at the different strain magnitudes was observed.

2.4 Equation of State

The platinum supercell with periodic boundary conditions was geometrically optimized using the conjugate gradient method and the temperature of the system was equilibrated at 298 K using a canonical ensemble for 3 ps. This was followed by a pressure-temperature equilibration process at 0.1 MPa (1 atm) and 298 K, using an isothermal-isobaric (NPT) ensemble for 5 ps. A Nosé-Hoover barostat was used to control the pressure of the system with a damping parameter of 1 ps.

After the equilibration process, the system was hydrostatically compressed in increments of 2 GPa to up to 50 GPa, while keeping the temperature constant. The discrete increments were enforced in an isothermal-isobaric ensemble for 2 ps and the systems were further equilibrated for 2 ps after each increment. The pressure P and volume V were time averaged over the last 0.5 ps of the equilibration run. Then, the bulk modulus was predicted by fitting the thermodynamic data to the Birch-Murnaghan equation of state [8, 64]

$$P(V) = \frac{3}{2}B_0 \left(\left(\frac{V}{V_0} \right)^{-\frac{7}{3}} - \left(\frac{V}{V_0} \right)^{-\frac{5}{3}} \right) \left(1 + \frac{3}{4}(B'_0 - 4) \left(\left(\frac{V}{V_0} \right)^{-\frac{2}{3}} - 1 \right) \right) \quad (3)$$

where V_0 is the initial volume, B_0 is the bulk modulus and B'_0 is the first derivative of the bulk modulus.

2.5 Stability of Small Pt Nanoparticles

The force fields described above were used to model 3.2 nm nanoparticles with cubic and icosahedral shapes. These shapes were selected because icosahedral and cubical platinum nanoparticles are stable, experimentally observed and theoretically predicted, [1] and because their facets are oriented in the $\{111\}$ and $\{100\}$ planes. Shrink-wrapped boundary conditions (i.e. the boundaries of the simulation box extended to the limits of the model system) were used for the simulations. The cube nanoparticles were generated using lammps and the icosahedral nanoparticles were generated with OpenMD. [43] The nanoparticles were geometrically optimized using the conjugate gradient method to achieve an energy convergence between steps of 1×10^{-7} . Next, the temperature was equilibrated at 298 K using a canonical ensemble for 0.3 ns. The stability of the nanoparticles was evaluated in terms of the change of potential energy over time. In addition to the Nosé-Hoover thermostat, the equilibration process was repeated with two different thermostats: Langevin and Berendsen. These additional simulations were performed to confirm that the performance of the force fields was independent of the thermostat.

3 Results and Discussion

Molecular dynamics simulations, using these nine different force fields, were used to calculate lattice constant, surface energies, stiffness constants, and bulk modulus derived from the equation of state of platinum. The results from each calculation are discussed below.

3.1 Lattice Constant

First, after a geometry optimization process and relaxation at room temperature and atmospheric pressure, the lattice constant for FCC platinum was calculated for each force field. The modeling results and standard deviation shown in Figure 1 are compared to the known experimental value of 0.392 nm. [56] It is observed that the predicted lattice constant of bulk platinum at room temperature, is close to the experimental value (error between 0.1% to 1.7%) for most of the force fields used in this work. The least accurate are the two REAX-(2014) and REAX-(2008) potentials that overestimate the lattice constant, but still have a small error of 0.9 and 1.7%, respectively. These differences can be explained by the parameterization of each force field. For the EAM and MEAM force fields, the lattice parameter is used as an input for the parameterization and so matches the experimental value almost exactly. However, ReaxFF is parameterized to match the atomic energies of a system, so larger variation of the lattice parameter can be expected.

Additionally, REAX-(2014) was parameterized to match DFT-calculated energies that predicted a lattice constant of 0.397 nm instead of the experimental value (0.392 nm). On the other hand, the REAX-(2008) parameterization was focused on matching the adsorption energy of platinum clusters on carbon platelets and not on the prediction of bulk properties. In the parameterization, [79] the lattice mismatch between the carbon and platinum atoms at the interface caused desorption of some platinum atoms and consequent restructuring of the atoms in the Pt cluster. These processes lead to longer Pt-Pt bonds and, consequently, a larger lattice parameter when the force field is used to simulate bulk platinum.

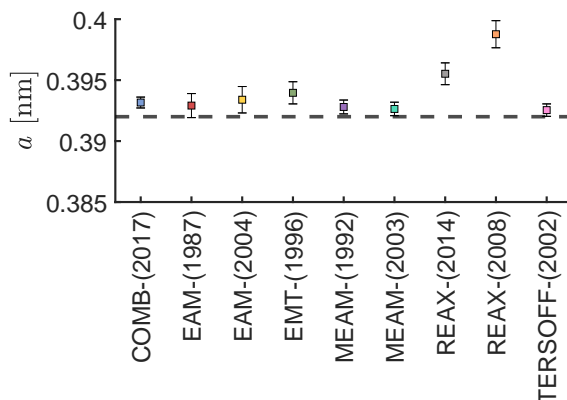


Figure 1: Lattice constant calculated by the force fields (symbols) compared to the experimental value (dashed line).

3.2 Surface Energies

Differences in the energies of the different surfaces are responsible for the stability of nanoparticles and favor the formation of specific geometric configurations. Experimental approaches to obtaining the surface energy of solids include calculations from contact angle measurements, [15] extrapolation for the solid phase from measurements of surface tension in a solid-liquid-vapor system, [93] and inverse gas chromatography, [68] among other methods. [20] Nevertheless, experimental calculation of the surface energy of specific facets is difficult and the results are often inconsistent among experiments. [92]

Quantum-mechanics calculations based on DFT have been widely used to calculate the surface energy of platinum. However, the calculated values are dependent on the exchange correlation function used and the selection of parameters. [94, 84] The general gradient approximation (GGA) tends to underestimate the surface energies, while the local density approximation (LDA) may overestimate it. Vega et al. [94] evaluated different DFT exchange correlation functionals and found that, although there are limitations, the Vosko-Wilk-Nusair (VWN) functional [96] within the local density approximation is well suited for predicting surface energies of platinum. In this study, we compare the energies predicted using different empirical potentials with the DFT values calculated by Vega et al. with the VWN functional.

Figure 2 shows the surface energies calculated using the different force fields evaluated in this work. The reference surface energy (DFT with the VWN functional) in each case (a) to (c) is shown as a dashed line. Additionally, energies reported from DFT calculations are shown as patterned areas. An extended literature review on the surface energies of platinum based on DFT and experimental results, and the values calculated from the nine force fields evaluated here are presented in the Supporting Information.

The EMT-(1996) potential severely underestimates the surface energy of all the faces, while the MEAM-(1992) potential calculates low surface energy for the (111) face. Surface energies calculated by the other potentials are within the range of values calculated using DFT with any exchange correlation function. Since the semi-empirical interatomic potentials are obtained by fitting to DFT values, the parameters predicted by the force fields likely correspond to the DFT approximation used in their parameterization.

Experimental surface energies are commonly calculated from measured liquid-metal surface tension and correspond to average surface energies over crystals with different face orientations, [74, 30] so Figure 2d shows the average of the surface energies in the three directions evaluated in this study compared to the range of experimental results. Although most force fields underestimate the surface energy, EAM-(2004), MEAM-(2003) and REAX-(2008) predict an average surface energy within the range of experimental values.

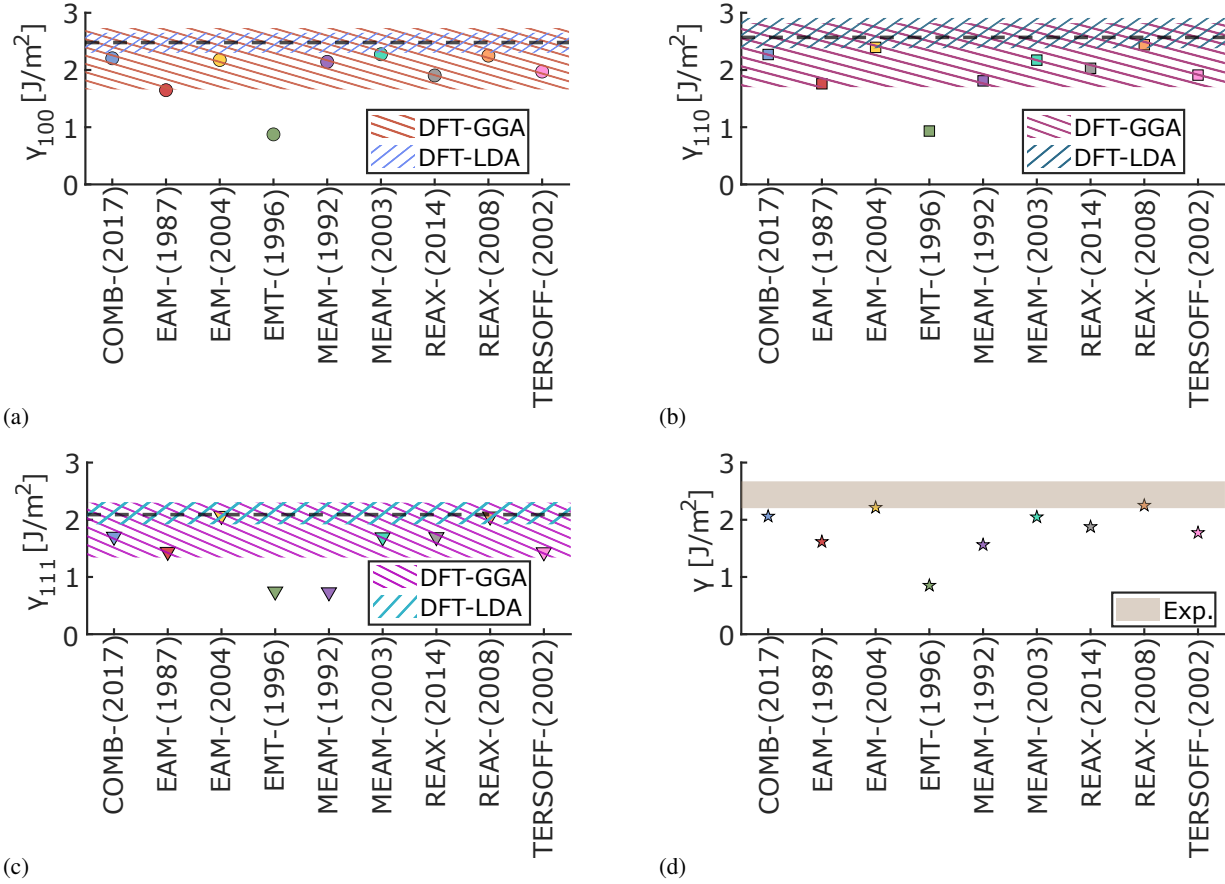


Figure 2: (a) γ_{100} , (b) γ_{110} , and (c) γ_{111} Surface energies from MD simulations (symbols) compared to DFT results (patterned areas). DFT values [94] calculated with the VWN functional are shown as dashed black lines. (d) Average surface energies γ from MD simulations (symbols) compared to experimental results (shaded area).

In general, the force fields are able to capture the differences between the energies of the different surfaces. Most MD-calculated surface energies follow $\gamma_{111} < \gamma_{100} < \gamma_{110}$, consistent with DFT and experimental results. An exception to this is observed for the MEAM-(1992) potential, where $\gamma_{100} > \gamma_{110}$ and, to a lesser extent, for the MEAM-Lee and TERSOFF-(2002) potentials, where γ_{100} is slightly larger than γ_{110} .

3.3 Stiffness Constants

The components of the stiffness tensor in Voigt notation [47] calculated by the different force fields are shown in Figure 3. All the force fields predict the orthotropy of platinum with C_{11} exactly equal to C_{22} and C_{33} , C_{13} equal to C_{23} and C_{12} , and C_{44} equal to C_{55} and C_{66} for the crystalline FCC Pt. The Zener anisotropy ratio $A = 2C_{44}/(C_{11} - C_{12})$ is also shown in Figure 3. The stiffness constant C_{44} represents resistance to shear on $\{100\}$ in $\langle 0kl \rangle$, while $C_{11} - C_{12}/2$ represents resistance to deformation by shear on $\{110\}$ in $\langle -110 \rangle$. Then, A represents the ratio of the extreme elastic-shear coefficients. For a perfectly isotropic medium, A has a value of 1. [58]

The two parametrizations of the REAX force field (2008) and (2014) underestimate the C_{12} constant, and overestimate C_{44} compared to the experimental values. The overestimation of C_{44} is more than two times the experimental constant and predicts that C_{44} is equal to C_{12} from both ReaxFF potentials. The relationship of shear response compared to dilation on compression is unrealistic for cubic crystals if C_{44} equals C_{12} , as it is shown also from the high value of the Zener ratio.

The original EAM-(1987) potential, the EMT potential, and the COMB potential also predict Zener anisotropic parameters that do not correspond to the experimental relation. Specifically, they predict a higher ratio between the elastic shear coefficients than that observed experimentally, corresponding to a larger degree of elastic anisotropy. By contrast, the EAM-(2004) potential, the Tersoff-like, and both MEAM potentials predict elastic properties very similar

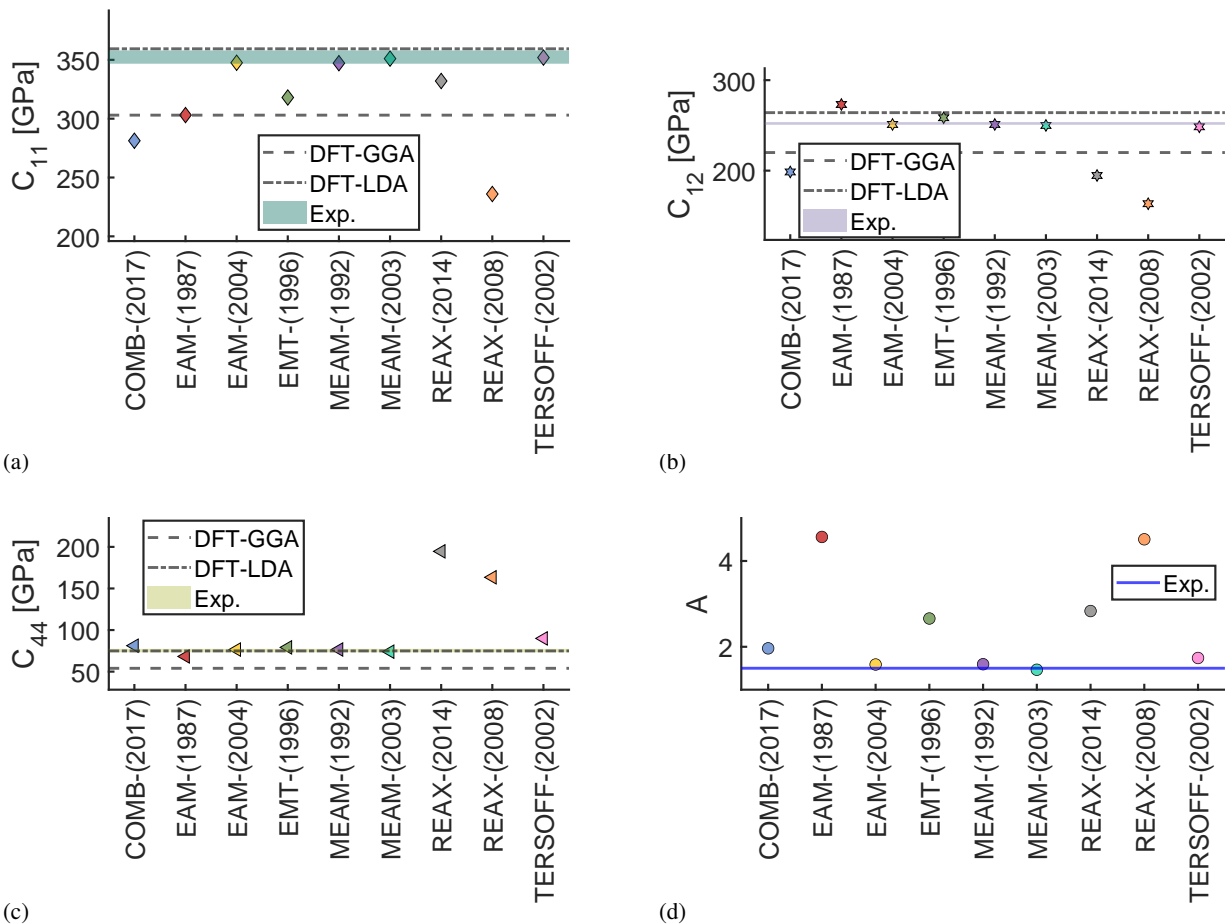


Figure 3: (a-c) Stiffness constants from MD simulations (symbols) compared to DFT [92, 63] (dashed lines) and experimental results (shaded areas) [82, 57] (a) C_{11} , (b) C_{12} , and (c) C_{44} . (d) Zener ratio A from MD simulations (symbols) compared to experimental results [82, 57] (blue line).

to experimental values. The calculated values of stiffness constants and elastic properties can be found in the Supporting Information.

3.4 Equation of State

Because of the small surface area of platinum nanoparticles, even low loads can exert large pressure. Therefore, a force field that accurately predicts volumetric changes in response to pressure is essential. Furthermore, erroneous phase changes estimated by the computational models reflect inaccurate energetic predictions of the potential and should be avoided.

The pressure-specific volume isotherms for platinum simulated with the nine different force fields selected for this study are shown in Figures 4a-c. Each figure shows isotherms predicted by three of the nine force fields compared to the curves from experimental studies. [50, 102] None of the predicted isotherms exhibits discontinuities except for the curve obtained using the MEAM-(1992) potential, shown in Figure 4b. Previous experimental [62] and DFT [89] studies have demonstrated that the pressure - specific volume isotherms for platinum do not diverge from the Birch-Murnaghan equation of state, even for pressures as high as 500 GPa, so the discontinuity observed for the MEAM-(1992) potential is unphysical.

The curves shown in Figure 4 were fitted to the Birch-Murnaghan equation of state from 0 GPa to 28 GPa, a range in which the isotherms are continuous for all the force fields. The isothermal bulk modulus B_0 and the first derivative of

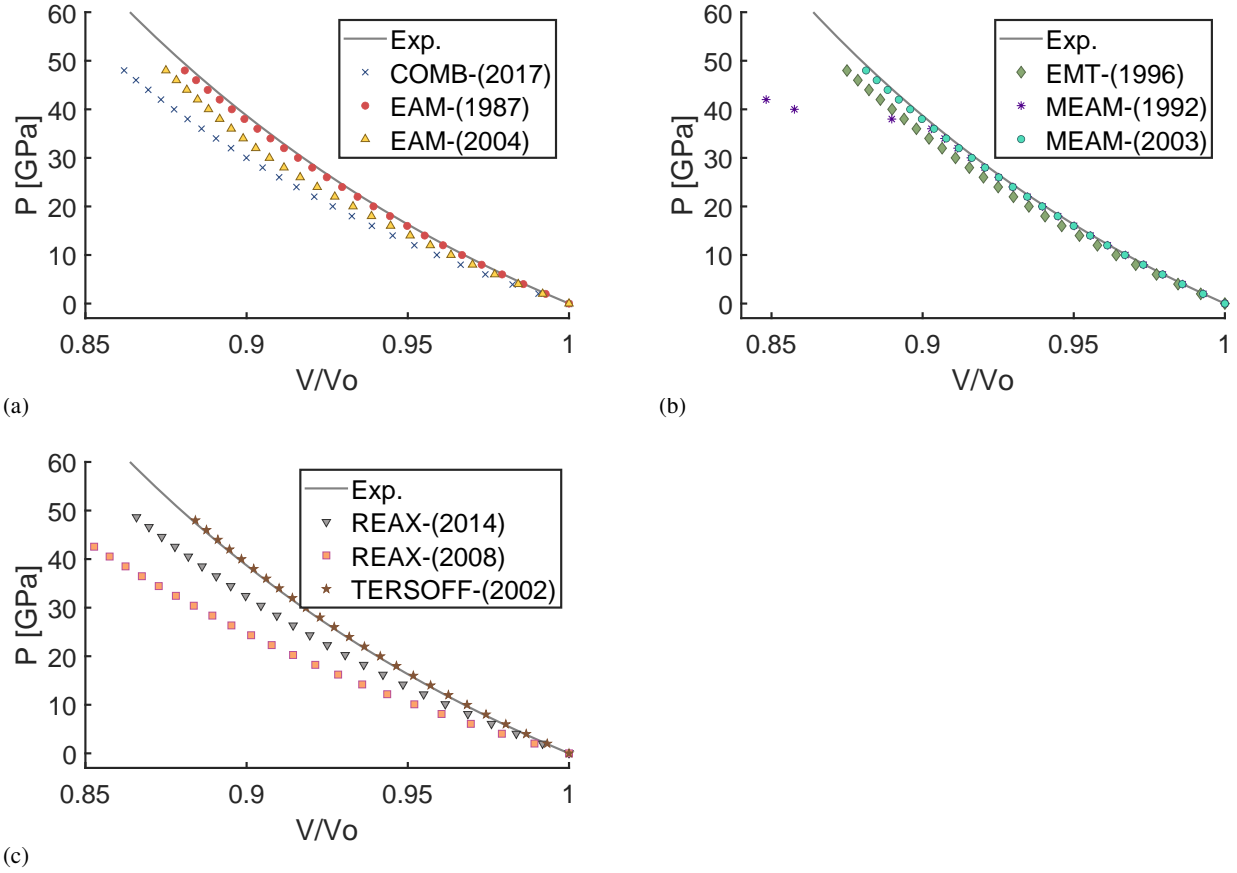


Figure 4: Pressure-volume (P-V) relationships for the different force fields (symbols) compared to experimental results [50, 102] (lines).

the bulk modulus B'_0 were obtained from the fit and reported in Figure 5. Calculated values and confidence bounds can be seen in the Supporting Information.

Results show that the bulk modulus derived from the equation of state is severely underestimated by the REAX-(2008) and the COMB-(2017) potentials. Previous studies of the equation of state of platinum based on DFT with the general gradient approximation, reported in the literature, [84, 25, 55] underestimate B_0 compared to experimental results. [62, 50, 102] The bulk modulus calculated with the EAM-(2004), EMT-(1996), and REAX-(2014) are similar to those properties calculated with DFT-GGA and the Perdew-Burke-Ernzerhof functional, [89] while the TERSOFF-(2002) potential overestimates the bulk modulus, similar to DFT-LDA calculations. [63] The bulk modulus calculated by the EAM-(1987), MEAM-(1992), and MEAM-(2003) are comparable to experimental values.

The pressure derivative of the bulk modulus quantifies the increased resistance to compression with increasing pressure. Figure 5b compares our simulation results with experimental values reported in the literature; the exact values are given in the Supporting Information (Table S5). The mean value of B'_0 for platinum is 5.2 ± 0.4 although there is a wide range of reported experimental values, likely because of differences in the chosen experimental method, the selection of fitted equation of state, [49] and the range of pressures evaluated. Most of the force fields evaluated are within the range of experimental measurements, except for EAM-(2004) which underestimates B'_0 , indicating that this force field less accurately predicts changes in the resistance to compression compared to the other potentials.

3.5 Force Field Selection

Bulk and surface properties of platinum calculated from the MD models with nine different force fields were compared to experimental results as detailed above: lattice parameter, [56] stiffness constants, [82, 57] and Birch-Murnaghan equation of state fit parameters (average of values reported in Refs. [32, 36, 106, 62, 103, 33, 102, 34]). The surface energies calculated from the MD models were compared to DFT calculations with the Vosko-Wilk-Nusair work

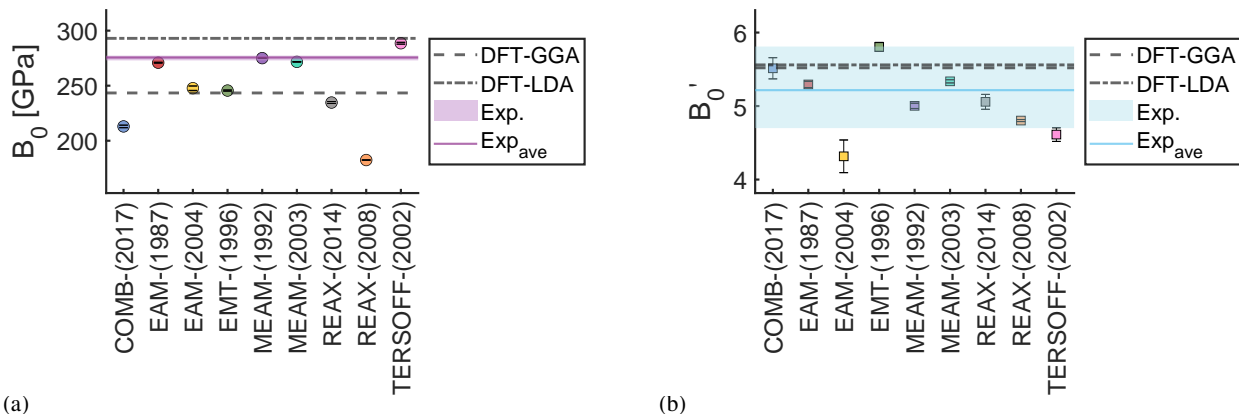


Figure 5: Bulk modulus at atmospheric pressure B_0 and its derivative B'_0 for platinum obtained by fitting pressure-volume data from different force fields in Figure 4 to the Birch-Murnaghan equation of state (symbols). Error bars reflect the 95%-confidence intervals. Results are compared to DFT values, [89, 92] shown as dash lines, and experimental results, [32, 36, 106, 62, 103, 33, 102, 34] shown as shaded areas. The average of the experimental results is shown as a solid line.

function. [94] To visualize the differences between the force fields and determine which is most accurate overall, radar plots were created, as shown in Figure 6. In these figures, a larger fill area means a smaller error, i.e. the perimeter of the radar plot corresponds to zero error, while the center point corresponds to 100% error. If the error was larger than 100%, the value was adjusted and is shown as a maximum error at the center point. The percentage of area filled was also calculated and is presented in these figures.

As seen in Figure 6, none of the nine evaluated potentials accurately predicts all the properties of platinum. There are uncertainties inherent to empirical force fields that are responsible for the inaccuracy. First, truncation in the calculation of short- and long-range interactions have to be assumed and are characteristics of the selected functional form of the force field. [3] Second, force field parameters are calibrated to reproduce specific experimental measurements and quantum mechanics calculations. However, when the potentials are used for simulations outside the scope of the conditions for which they were parameterized, their predictions may become inaccurate. [3] Additionally, because of the fit to experimental measurements, the parameterization of a force field is susceptible to experimental or observational errors. There are also differences in the material models employed in MD compared to real materials in experiments. In our MD models, the simulated material is based on a perfect crystal, while in reality materials are affected by defects, grain distribution and size, or grain boundary effects. Finally, force field parameters fitted to DFT results depend heavily on the approximation to the exchange correlation energy functional chosen for the DFT calculations and fitting.

Regardless, visual analysis of Fig. 6 indicates that the COMB-(2017), EAM-(2004), MEAM-(2003), MEAM (1992), and TERSOFF-(2002) force fields are the most accurate in terms of their ability to model physical and mechanical properties of platinum in its bulk form using periodic boundary conditions, for pressures up to 28 GPa. This observation is supported quantitatively by the percentage of the total radar plot area filled, which is above 75% for the above-mentioned five force fields. However, molecular models of nanomaterials have features not present in bulk materials due to the lack of neighboring atoms at the surface of the systems and differences in the boundary conditions of the simulation cell. Therefore, the potentials were further evaluated based on the stability of nanoparticles with facets in different orientations, as presented next.

3.6 Stability of Small Platinum Nanoparticles

A cubic platinum nanoparticle with $\{100\}$ facets and an icosahedral nanoparticle with $\{111\}$ facets were evaluated. An initial geometric optimization showed that the displacement of the surface atoms differed from the displacement of the subsurface atoms relative to their initial positions. Representative snapshots from the optimization with atoms colored according to their atomic displacement are shown in Figure 7a for the cubic nanoparticle and Figure 8a for the icosahedral nanoparticle, with visualization performed using OVITO software. [88] The direction of this atomic displacement followed the same pattern for all the potentials, except for the cubic nanoparticle with both ReaxFF (figures for all the force fields shown in Supporting Information). For most of the force fields, the optimized positions of the subsurface atoms corresponded to the crystalline FCC phase, while the atoms at the surface moved slightly

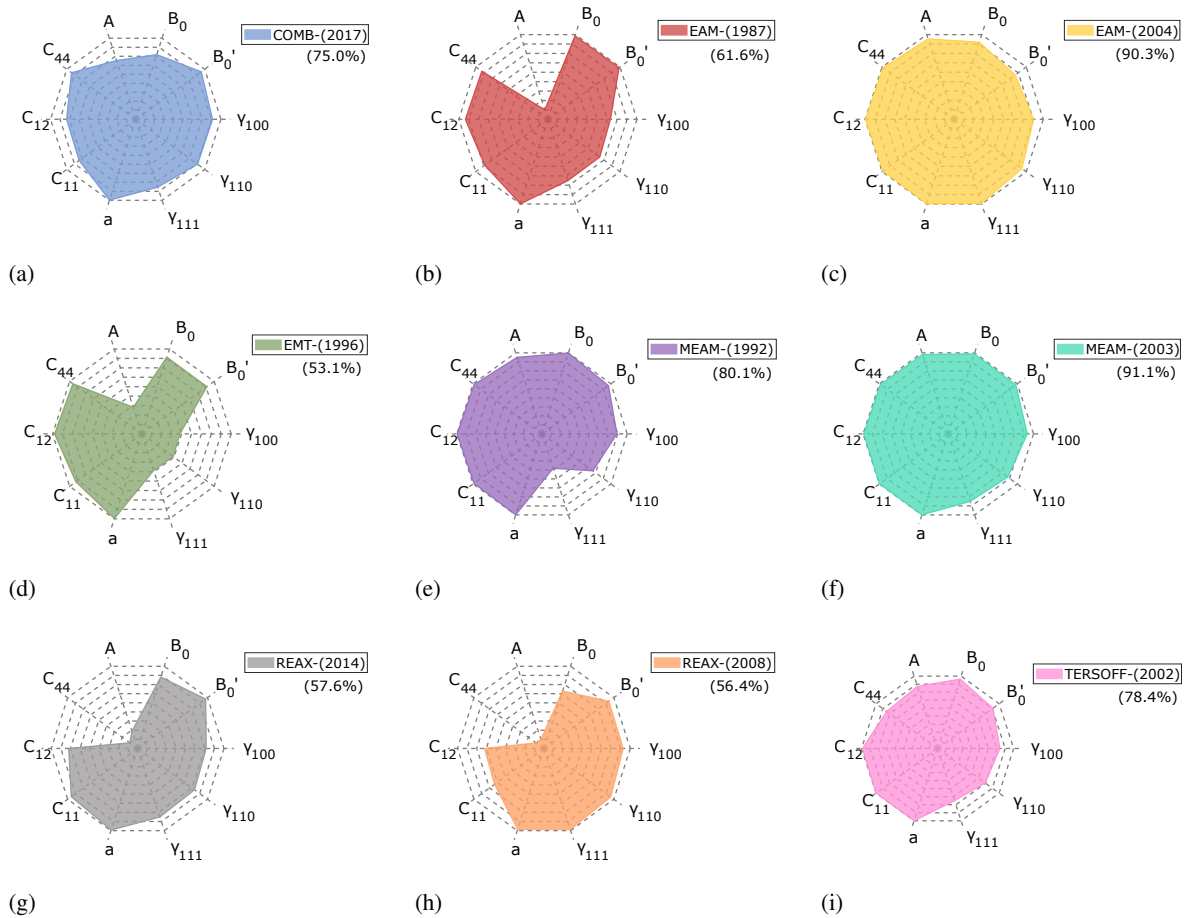


Figure 6: Radar plots summarizing the accuracy of MD calculations based on comparisons to experimental values and DFT calculations: (a) COMB-(2017), (b) EAM-(1987), (c) EAM-(2004), (d) EMT-(1996), (e) MEAM-(1992), (f) MEAM-(2003), (g) REAX-(2014), (h) REAX-(2008), and (i) TERSOFF-(2002). The percentage of the radar plot area filled, given in parenthesis, quantifies overall accuracy, where a higher percentage reflects greater accuracy.

inward as a result of the energy imbalance from the lack of neighboring atoms. Different behavior was observed for the cubic nanoparticle with both ReaxFF potentials, where the surface atoms remained near their initial positions, and the subsurface atoms moved towards the surface. However, the final configurations for all the force fields had internal atoms corresponding to the crystalline FCC phase and surface atoms displaced from the FCC lattice. This effect was more pronounced at the corners and edges of the structures.

Following geometry optimization, the nanoparticles were equilibrated at room temperature for 0.3 ns. The stability of the nanoparticle was then evaluated based on the change in potential energy over time, i.e. the potential energy will have small fluctuations around a constant mean value if the structure is stable.

Figure 7 shows the potential energy per atom of the cubic nanoparticle with faces oriented in $\{100\}$ planes during the thermal equilibration process. For all force fields except MEAM-(2003), the cubic nanoparticle is stable at room temperature. With the MEAM-(2003) potential, the potential energy decreases with increasing equilibration time, indicating continuous structural reordering over time. In contrast, all the other potentials show an initial relaxation of the potential energy followed by stability of the nanoparticle in a cubic form. Studies on platinum nanoparticles have shown that nanocubes can be synthesized and are stable at room temperature. [100, 41]

Figure 8 shows the potential energy per atom vs equilibration time for the icosahedral nanoparticle with facets oriented in $\{111\}$ planes. All the force fields predict stable icosahedral nanoparticles, except the MEAM-(1992) force field which exhibits a sudden change in the potential energy without external disturbance. Synthesis of stable icosahedral nanoparticles has been proven to be feasible experimentally. [100]

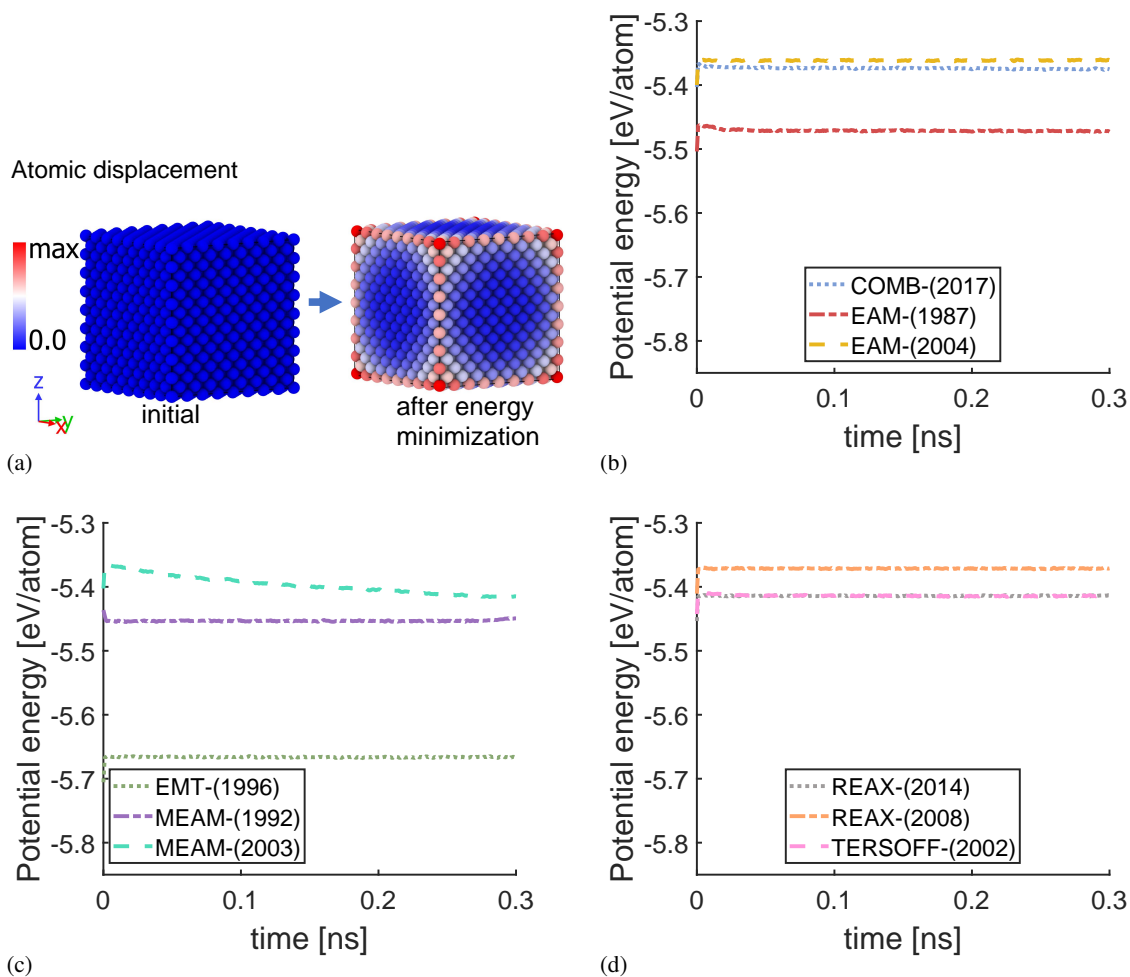


Figure 7: (a) Representative snapshot of a 3.2 nm cubic nanoparticle before and after energy minimization with atom colors corresponding to displacement in 10^{-1} nm. (b)-(d) Potential energy per atom during thermal equilibration with the different force fields.

The prediction of nanoparticle stability was evaluated using three different thermostats. The results with the Nosé-Hoover thermostat are shown in figures 7 and 8, but the same trends are exhibited by the other thermostats, as shown in the Supporting Information, Figures S4-S7. With all three thermostats, the MEAM-(2003) force field predicts an unstable cube with facets in $\{100\}$ orientations and the MEAM-(1992) predicts unstable icosahedron with facets in $\{111\}$ orientations, while the other force fields predict stable nanoparticles. This analysis of the stability of nanoparticles demonstrates that the MEAM-(1992) and the MEAM-(2003) force fields are not suitable for modeling faceted platinum nanoparticles, although the MEAM-(2003) accurately predicted the properties of bulk platinum.

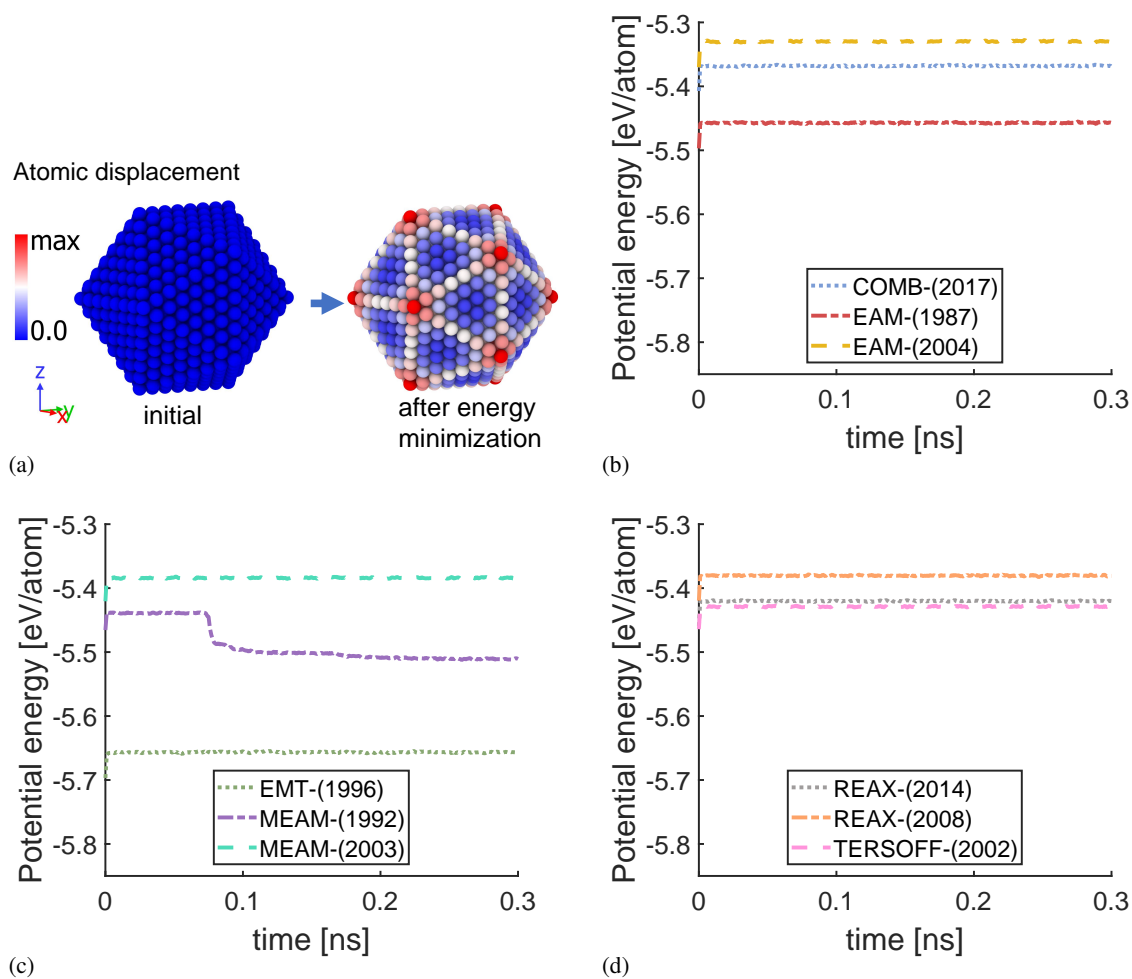


Figure 8: a) Representative snapshot of a 3.2 nm icosahedral nanoparticle before and after energy minimization with atom colors corresponding to displacement in 10^{-1} nm. (b)-(d) Potential energy per atom during thermal equilibration with the different force fields.

4 Conclusions

In this study, we evaluated the ability of nine potentials to model small, faceted platinum nanoparticles using molecular dynamics simulations. First, the force fields were evaluated based on their prediction of bulk and surface properties, specifically: stiffness constants, the equation of state, and surface energies. The simulation-predicted values were compared to results from experiments or quantum mechanics calculations. Five force fields, the EAM-(2004), [108] MEAM-(2003), [59], MEAM-(1992), 6, Tersoff-(2002), [2], and COMB-(2017) [4] potentials were found to be the most accurate in terms of their ability to model physical, mechanical and surface properties. However, the MEAM-(1992) force field is not recommended to model systems with pressures above 28 GPa. Further, an analysis of the stability of nanoparticles with surfaces in the {100} and {111} planes revealed that the MEAM-(2003) and MEAM-(1992) potentials failed to reproduce the structural integrity of nanoparticles that can be synthesized and remain stable at room conditions in experimental conditions. The EAM-(2004) potential, the Tersoff-(2002) potential, and the COMB-(2017) potential predicted the expected nanoparticle stability. Therefore, since the bulk and surface properties were most accurately predicted by the EAM-(2004) potential, [108] this study demonstrates that this EAM potential is the most suitable for molecular dynamics simulations of small, faceted platinum nanoparticles.

4.1 Acknowledgement

This material is based upon work supported by the U.S. Department of Energy, Office of Science, Office of Basic Energy Sciences, under Award Number DE-FOA-0002181. Some of the simulations were run using the Extreme Science and Engineering Discovery Environment (XSEDE), which is supported by the National Science Foundation Grant ACI-1548562.

4.2 Supporting Information

The representation of a slab system for calculation of surface energies, a comprehensive review of the surface energy of platinum and bulk modulus derived from the equation of state, calculated bulk and surface properties, and the atomic displacement for the two nanoparticles shapes after energy minimization process are available in the Supporting Information.

References

- [1] M. Ahmadi, J. Timoshenko, F. Behafarid, and B. Roldan Cuenya. Tuning the Structure of Pt Nanoparticles through Support Interactions: An in Situ Polarized X-ray Absorption Study Coupled with Atomistic Simulations. *J. Phys. Chem. C*, 123(16):10666–10676, mar 2019. doi:10.1021/acs.jpcc.9b00945.
- [2] K. Albe, K. Nordlund, and R. S. Averback. Modeling the metal-semiconductor interaction: Analytical bond-order potential for platinum-carbon. *Phys. Rev. B*, 65(19):195124, may 2002. doi:10.1103/PhysRevB.65.195124. URL <https://link.aps.org/doi/10.1103/PhysRevB.65.195124>.
- [3] P. Angelikopoulos, C. Papadimitriou, and P. Koumoutsakos. Bayesian uncertainty quantification and propagation in molecular dynamics simulations: A high performance computing framework. *J. Chem. Phys.*, 137(14):144103, oct 2012. ISSN 0021-9606. doi:10.1063/1.4757266. URL <https://doi.org/10.1063/1.4757266>.
- [4] A. C. Antony, S. A. Akhade, Z. Lu, T. Liang, M. J. Janik, S. R. Phillpot, and S. B. Sinnott. Charge optimized many body (COMB) potentials for Pt and Au. *J. Phys.: Condens. Matter*, 29(22):225901, jun 2017. doi:10.1088/1361-648X/aa6d43. URL <https://iopscience.iop.org/article/10.1088/1361-648X/aa6d43>.
- [5] J. N. Armor. A history of industrial catalysis. *Catal. Today*, 163(1):3–9, 2011. ISSN 0920-5861. doi:<https://doi.org/10.1016/j.cattod.2009.11.019>. URL <http://www.sciencedirect.com/science/article/pii/S0920586109006944>.
- [6] M. I. Baskes. Modified embedded-atom potentials for cubic materials and impurities. *Phys. Rev. B*, 46(5):2727–2742, aug 1992. doi:10.1103/PhysRevB.46.2727. URL <https://link.aps.org/doi/10.1103/PhysRevB.46.2727>.
- [7] M. I. Baskes and C. F. Melius. Pair potentials for fcc metals. *Phys. Rev. B*, 20(8):3197–3204, oct 1979. doi:10.1103/PhysRevB.20.3197. URL <https://link.aps.org/doi/10.1103/PhysRevB.20.3197>.
- [8] F. Birch. Finite Elastic Strain of Cubic Crystals. *Phys. Rev.*, 71(11):809–824, jun 1947. doi:10.1103/PhysRev.71.809. URL <https://link.aps.org/doi/10.1103/PhysRev.71.809>.
- [9] D. W. Brenner. Empirical potential for hydrocarbons for use in simulating the chemical vapor deposition of diamond films. *Phys. Rev. B*, 42(15):9458–9471, nov 1990. doi:10.1103/PhysRevB.42.9458. URL <https://link.aps.org/doi/10.1103/PhysRevB.42.9458>.

- [10] D. Brondani, C. W. Scheeren, J. Dupont, and I. C. Vieira. Biosensor based on platinum nanoparticles dispersed in ionic liquid and laccase for determination of adrenaline. *Sens. Actuators. B*, 140(1):252–259, 2009. ISSN 0925-4005. doi:<https://doi.org/10.1016/j.snb.2009.04.037>. URL <http://www.sciencedirect.com/science/article/pii/S0925400509003475>.
- [11] A. Bruix, J. A. Rodriguez, P. J. Ramírez, S. D. Senanayake, J. Evans, J. B. Park, D. Stacchiola, P. Liu, J. Hrbek, and F. Illas. A new type of strong metal–support interaction and the production of h₂ through the transformation of water on pt/ceo₂(111) and pt/ceox/tio₂(110) catalysts. *J. Am. Chem. Soc.*, 134(21):8968–8974, 2012. doi:10.1021/ja302070k. URL <https://doi.org/10.1021/ja302070k>. PMID: 22563752.
- [12] A. C. T. van Duin, S. Dasgupta, F. Lorant, and W. A. Goddard. ReaxFF: A Reactive Force Field for Hydrocarbons. *J. Phys. Chem. A*, 105(41):9396–9409, sep 2001. doi:10.1021/jp004368u.
- [13] J. Cai and Y. Y. Ye. Simple analytical embedded-atom-potential model including a long-range force for fcc metals and their alloys. *Phys. Rev. B*, 54(12):8398–8410, sep 1996. doi:10.1103/PhysRevB.54.8398. URL <https://link.aps.org/doi/10.1103/PhysRevB.54.8398>.
- [14] G. Calogero, P. Calandra, A. Irrera, A. Sinopoli, I. Citro, and G. Di Marco. A new type of transparent and low cost counter-electrode based on platinum nanoparticles for dye-sensitized solar cells. *Energy Environ. Sci.*, 4(5):1838–1844, 2011. ISSN 1754-5692. doi:10.1039/C0EE00463D. URL <http://dx.doi.org/10.1039/C0EE00463D>.
- [15] A. Calvimontes. The measurement of the surface energy of solids using a laboratory drop tower. *npj Microgravity*, 3(1):25, 2017. ISSN 2373-8065. doi:10.1038/s41526-017-0031-y. URL <https://doi.org/10.1038/s41526-017-0031-y>.
- [16] S. Cao, J. Jiang, B. Zhu, and J. Yu. Shape-dependent photocatalytic hydrogen evolution activity over a Pt nanoparticle coupled g-C₃N₄ photocatalyst. *Phys. Chem. Chem. Phys.*, 18(28):19457–19463, 2016. ISSN 1463-9076. doi:10.1039/C6CP02832B. URL <http://dx.doi.org/10.1039/C6CP02832B>.
- [17] A. Caro, D. A. Crowson, and M. Caro. Classical Many-Body Potential for Concentrated Alloys and the Inversion of Order in Iron-Chromium Alloys. *Phys. Rev. Lett.*, 95(7):75702, aug 2005. doi:10.1103/PhysRevLett.95.075702. URL <https://link.aps.org/doi/10.1103/PhysRevLett.95.075702>.
- [18] G. Casillas, J. P. Palomares-Báez, J. L. Rodríguez-López, J. Luo, A. Ponce, R. Esparza, J. J. Velázquez-Salazar, A. Hurtado-Macias, J. González-Hernández, and M. José-Yacaman. In situ TEM study of mechanical behaviour of twinned nanoparticles. *Philos. Mag.*, 92(35):4437–4453, dec 2012. ISSN 1478-6435. doi:10.1080/14786435.2012.709951. URL <https://doi.org/10.1080/14786435.2012.709951>.
- [19] J. Chapman and R. Ramprasad. Multiscale Modeling of Defect Phenomena in Platinum Using Machine Learning of Force Fields. *JOM*, 72(12):4346–4358, 2020. ISSN 1543-1851. doi:10.1007/s11837-020-04385-0. URL <https://doi.org/10.1007/s11837-020-04385-0>.
- [20] P. Chen, Y. Gao, and M. R. Castell. Experimental determination of the {111}/{001} surface energy ratio for Pd crystals. *Appl. Phys. Lett.*, 117(10):101601, sep 2020. ISSN 0003-6951. doi:10.1063/5.0022879. URL <https://doi.org/10.1063/5.0022879>.
- [21] I. V. Chepkasov, M. A. Visotin, E. A. Kovaleva, A. M. Manakhov, V. S. Baidyshev, and Z. I. Popov. Stability and Electronic Properties of PtPd Nanoparticles via MD and DFT Calculations. *J. Phys. Chem. C*, 122(31):18070–18076, aug 2018. ISSN 1932-7447. doi:10.1021/acs.jpcc.8b04177. URL <https://doi.org/10.1021/acs.jpcc.8b04177>.
- [22] C.-Y. Chiu, Y. Li, L. Ruan, X. Ye, C. B. Murray, and Y. Huang. Platinum nanocrystals selectively shaped using facet-specific peptide sequences. *Nat. Chem.*, 3(5):393–399, 2011. ISSN 1755-4349. doi:10.1038/nchem.1025. URL <https://doi.org/10.1038/nchem.1025>.
- [23] S. Choi, M. Chung, D. Kim, S. Kim, K. Yun, W. Cha, R. Harder, T. Kawaguchi, Y. Liu, A. Ulvestad, H. You, M. K. Song, and H. Kim. In Situ Strain Evolution on Pt Nanoparticles during Hydrogen Peroxide Decomposition. *Nano Lett.*, 20(12):8541–8548, dec 2020. ISSN 1530-6984. doi:10.1021/acs.nanolett.0c03005. URL <https://doi.org/10.1021/acs.nanolett.0c03005>.
- [24] F. Cleri and V. Rosato. Tight-binding potentials for transition metals and alloys. *Phys. Rev. B*, 48(1):22–33, jul 1993. doi:10.1103/PhysRevB.48.22. URL <https://link.aps.org/doi/10.1103/PhysRevB.48.22>.
- [25] J. L. F. Da Silva, C. Stampfl, and M. Scheffler. Converged properties of clean metal surfaces by all-electron first-principles calculations. *Surf. Sci.*, 600(3):703–715, 2006. ISSN 0039-6028. doi:<https://doi.org/10.1016/j.susc.2005.12.008>. URL <http://www.sciencedirect.com/science/article/pii/S0039602805013154>.

- [26] X. D. Dai, Y. Kong, J. H. Li, and B. X. Liu. Extended Finnis–Sinclair potential for bcc and fcc metals and alloys. *J. Phys.: Condens. Matter*, 18(19):4527–4542, may 2006. ISSN 0953-8984. doi:10.1088/0953-8984/18/19/008. URL <https://iopscience.iop.org/article/10.1088/0953-8984/18/19/008>.
- [27] T. Daio, A. Staykov, L. Guo, J. Liu, M. Tanaka, S. Matthew Lyth, and K. Sasaki. Lattice Strain Mapping of Platinum Nanoparticles on Carbon and SnO₂ Supports. *Sci. Rep.*, 5(1):13126, 2015. ISSN 2045-2322. doi:10.1038/srep13126. URL <https://doi.org/10.1038/srep13126>.
- [28] M. S. Daw and M. I. Baskes. Semiempirical, Quantum Mechanical Calculation of Hydrogen Embrittlement in Metals. *Phys. Rev. Lett.*, 50(17):1285–1288, apr 1983. doi:10.1103/PhysRevLett.50.1285. URL <https://link.aps.org/doi/10.1103/PhysRevLett.50.1285>.
- [29] A. De Clercq, S. Giorgio, and C. Mottet. Pd surface and Pt subsurface segregation in Pt_{1-c}Pd_c nanoalloys. *J. Phys.: Condens. Matter*, 28(6):064006, feb 2016. ISSN 0953-8984. doi:10.1088/0953-8984/28/6/064006. URL <https://iopscience.iop.org/article/10.1088/0953-8984/28/6/064006>.
- [30] S. De Waele, K. Lejaeghere, M. Sluydts, and S. Cottenier. Error estimates for density-functional theory predictions of surface energy and work function. *Phys. Rev. B*, 94:235418, Dec 2016. doi:10.1103/PhysRevB.94.235418. URL <https://link.aps.org/doi/10.1103/PhysRevB.94.235418>.
- [31] J. Deneen Nowak, W. M. Mook, A. M. Minor, W. W. Gerberich, and C. B. Carter. Fracturing a nanoparticle. *Philos. Mag.*, 87(1):29–37, jan 2007. ISSN 1478-6435. doi:10.1080/14786430600876585. URL <https://doi.org/10.1080/14786430600876585>.
- [32] A. Dewaele, P. Loubeyre, and M. Mezouar. Equations of state of six metals above 94 GPa. *Phys. Rev. B*, 70:094112, Sep 2004. doi:10.1103/PhysRevB.70.094112. URL <https://link.aps.org/doi/10.1103/PhysRevB.70.094112>.
- [33] S. M. Dorfman, V. B. Prakapenka, Y. Meng, and T. S. Duffy. Intercomparison of pressure standards (Au, Pt, Mo, MgO, NaCl and Ne) to 2.5 Mbar. *J Geophys Res-Sol EA*, 117, AUG 30 2012. ISSN 2169-9313. doi:10.1029/2012JB009292.
- [34] V. M. Elkin, V. N. Mikhaylov, A. A. Ovechkin, and N. A. Smirnov. A wide-range multiphase equation of state for platinum. *J Phys-Condens Mat*, 32(43):435403, oct 2020. ISSN 0953-8984. doi:10.1088/1361-648X/aba428. URL <https://iopscience.iop.org/article/10.1088/1361-648X/aba428>.
- [35] D. Fantauzzi, J. Bandlow, L. Sabo, J. E. Mueller, A. C. T. van Duin, and T. Jacob. Development of a reaxff potential for pt–o systems describing the energetics and dynamics of pt-oxide formation. *Phys. Chem. Chem. Phys.*, 16(42):23118–23133, 2014. doi:10.1039/C4CP03111C. URL <http://dx.doi.org/10.1039/C4CP03111C>.
- [36] Y. Fei, J. Li, K. Hirose, W. Minarik, J. Van Orman, C. Sanloup, W. van Westrenen, T. Komabayashi, and K. ichi Funakoshi. A critical evaluation of pressure scales at high temperatures by in situ x-ray diffraction measurements. *Phys Earth Planet In*, 143-144:515–526, 2004. ISSN 0031-9201. doi:https://doi.org/10.1016/j.pepi.2003.09.018. URL <https://www.sciencedirect.com/science/article/pii/S0031920104000858>. New Developments in High-Pressure Mineral Physics and Applications to the Earth’s Interior.
- [37] M. W. Finnis and J. E. Sinclair. A simple empirical N-body potential for transition metals. *Philos. Mag. A*, 50(1):45–55, jul 1984. ISSN 0141-8610. doi:10.1080/01418618408244210. URL <https://doi.org/10.1080/01418618408244210>.
- [38] H. A. Firouzjaie and W. E. Mustain. Catalytic Advantages, Challenges, and Priorities in Alkaline Membrane Fuel Cells. *ACS Catal.*, 10(1):225–234, jan 2020. doi:10.1021/acscatal.9b03892. URL <https://doi.org/10.1021/acscatal.9b03892>.
- [39] S. M. Foiles. Reconstruction of fcc (110) surfaces. *Surf. Sci.*, 191(1):L779–L786, 1987. ISSN 0167-2584. doi:https://doi.org/10.1016/0167-2584(87)90889-9. URL <http://www.sciencedirect.com/science/article/pii/0167258487908899>.
- [40] S. M. Foiles, M. I. Baskes, and M. S. Daw. Embedded-atom-method functions for the fcc metals Cu, Ag, Au, Ni, Pd, Pt, and their alloys. *Phys. Rev. B*, 33(12):7983–7991, jun 1986. doi:10.1103/PhysRevB.33.7983. URL <https://link.aps.org/doi/10.1103/PhysRevB.33.7983>.
- [41] G. Fu, K. Wu, X. Jiang, L. Tao, Y. Chen, J. Lin, Y. Zhou, S. Wei, Y. Tang, T. Lu, and X. Xia. Polyallylamine-directed green synthesis of platinum nanocubes. shape and electronic effect codependent enhanced electrocatalytic activity. *Phys. Chem. Chem. Phys.*, 15:3793–3802, 2013. doi:10.1039/C3CP44191A. URL <http://dx.doi.org/10.1039/C3CP44191A>.
- [42] B. Garlyyev, K. Kratzl, M. Rück, J. Michalička, J. Fichtner, J. M. Macak, T. Kratky, S. Günther, M. Cokoja, A. S. Bandarenka, A. Gagliardi, and R. A. Fischer. Optimizing the size of platinum nanoparticles for enhanced mass activity in the electrochemical oxygen reduction reaction. *Angew. Chem., Int. Ed.*, 58(28):9596–9600,

2019. doi:<https://doi.org/10.1002/anie.201904492>. URL <https://onlinelibrary.wiley.com/doi/abs/10.1002/anie.201904492>.
- [43] J. Gezelter, S. Kuang, J. Marr, K. Stocker, C. Li, C. Vardeman, T. Lin, C. Fennell, X. Sun, K. Daily, et al. Openmd, an open source engine for molecular dynamics. *University of Notre Dame, Notre Dame, IN*, 2010.
- [44] O. D. Häberlen, S.-C. Chung, M. Stener, and N. Rösch. From clusters to bulk: A relativistic density functional investigation on a series of gold clusters Aun, n=6,...,147. *J. Chem. Phys.*, 106(12):5189–5201, mar 1997. ISSN 0021-9606. doi:10.1063/1.473518. URL <https://doi.org/10.1063/1.473518>.
- [45] L. M. Hale, Z. T. Trautt, and C. A. Becker. Evaluating variability with atomistic simulations: The effect of potential and calculation methodology on the modeling of lattice and elastic constants. *Modell. Simul. Mater. Sci. Eng.*, 26(5), may 2018. ISSN 1361651X. doi:10.1088/1361-651X/aabc05.
- [46] J. A. Harrison, J. D. Schall, S. Maskey, P. T. Mikulski, M. T. Knippenberg, and B. H. Morrow. Review of force fields and intermolecular potentials used in atomistic computational materials research. *Appl. Phys. Rev.*, 5(3): 31104, aug 2018. doi:10.1063/1.5020808. URL <https://doi.org/10.1063/1.5020808>.
- [47] R. F. S. Hearmon. The elastic constants of anisotropic materials. *Rev. Mod. Phys.*, 18:409–440, Jul 1946. doi:10.1103/RevModPhys.18.409. URL <https://link.aps.org/doi/10.1103/RevModPhys.18.409>.
- [48] A. Hernandez, A. Balasubramanian, F. Yuan, S. A. M. Mason, and T. Mueller. Fast, accurate, and transferable many-body interatomic potentials by symbolic regression. *npj Comput. Mater.*, 5(1):112, 2019. ISSN 2057-3960. doi:10.1038/s41524-019-0249-1. URL <https://doi.org/10.1038/s41524-019-0249-1>.
- [49] A. M. Hofmeister. Pressure derivatives of the bulk modulus. *J. Geophys Res-Sol EA*, 96(B13):21893–21907, 1991. doi:<https://doi.org/10.1029/91JB02157>. URL <https://agupubs.onlinelibrary.wiley.com/doi/abs/10.1029/91JB02157>.
- [50] N. C. Holmes, J. A. Moriarty, G. R. Gathers, and W. J. Nellis. The equation of state of platinum to 660 GPa (6.6 Mbar). *J. Appl. Phys.*, 66(7):2962–2967, oct 1989. ISSN 0021-8979. doi:10.1063/1.344177. URL <https://doi.org/10.1063/1.344177>.
- [51] K. W. Jacobsen, J. K. Nørskov, and M. J. Puska. Interatomic interactions in the effective-medium theory. *Phys. Rev. B*, 35(14):7423–7442, may 1987. doi:10.1103/PhysRevB.35.7423. URL <https://link.aps.org/doi/10.1103/PhysRevB.35.7423>.
- [52] K. W. Jacobsen, P. Stoltze, and J. K. Nørskov. A semi-empirical effective medium theory for metals and alloys. *Surf. Sci.*, 366(2):394–402, 1996. ISSN 0039-6028. doi:[https://doi.org/10.1016/0039-6028\(96\)00816-3](https://doi.org/10.1016/0039-6028(96)00816-3). URL <http://www.sciencedirect.com/science/article/pii/0039602896008163>.
- [53] A. Januszko and S. K. Bose. Phonon spectra and temperature variation of bulk properties of Cu, Ag, Au and Pt using Sutton–Chen and modified Sutton–Chen potentials. *J. Phys. Chem. Solids*, 82:67–75, 2015. ISSN 0022-3697. doi:<https://doi.org/10.1016/j.jpcs.2015.03.008>. URL <http://www.sciencedirect.com/science/article/pii/S0022369715000633>.
- [54] C. K. Jung, L. Braunwarth, and T. Jacob. Grand Canonical ReaxFF Molecular Dynamics Simulations for Catalytic Reactions. *J. Chem. Theory Comput.*, 15(11):5810–5816, nov 2019. ISSN 1549-9618. doi:10.1021/acs.jctc.9b00687. URL <https://doi.org/10.1021/acs.jctc.9b00687>.
- [55] A. Khein, D. J. Singh, and C. J. Umrigar. All-electron study of gradient corrections to the local-density functional in metallic systems. *Phys. Rev. B*, 51(7):4105–4109, feb 1995. doi:10.1103/PhysRevB.51.4105. URL <https://link.aps.org/doi/10.1103/PhysRevB.51.4105>.
- [56] C. Kittel. *Introduction to solid state physics*. Wiley, Hoboken, NJ, 2005. ISBN 047141526X 9780471415268 0471680575 9780471680574.
- [57] H. Landolt, K. H. Hellwege, R. Bornstein, and O. Madelung. *Landolt-Bornstein numerical data and functional relationships in science and technology. Group III., Group III.,.* Springer-Verlag, Berlin, 1966.
- [58] H. Ledbetter and A. Migliori. A general elastic-anisotropy measure. *J. Appl. Phys.*, 100(6):63516, sep 2006. ISSN 0021-8979. doi:10.1063/1.2338835. URL <https://doi.org/10.1063/1.2338835>.
- [59] B.-J. Lee, J.-H. Shim, and M. I. Baskes. Semiempirical atomic potentials for the fcc metals Cu, Ag, Au, Ni, Pd, Pt, Al, and Pb based on first and second nearest-neighbor modified embedded atom method. *Phys. Rev. B*, 68(14):144112, oct 2003. doi:10.1103/PhysRevB.68.144112. URL <https://link.aps.org/doi/10.1103/PhysRevB.68.144112>.
- [60] Y. Li, J. Petroski, and M. A. El-Sayed. Activation energy of the reaction between hexacyanoferrate(iii) and thiosulfate ions catalyzed by platinum nanoparticles. *J. Phys. Chem. B*, 104(47):10956–10959, 2000. doi:10.1021/jp002569s. URL <https://doi.org/10.1021/jp002569s>.

- [61] J. Ludwig, D. G. Vlachos, A. C. T. van Duin, and W. A. Goddard. Dynamics of the Dissociation of Hydrogen on Stepped Platinum Surfaces Using the ReaxFF Reactive Force Field. *J. Phys. Chem. B*, 110(9):4274–4282, feb 2006. doi:10.1021/jp0561064.
- [62] M. Matsui, E. Ito, T. Katsura, D. Yamazaki, T. Yoshino, A. Yokoyama, and K.-i. Funakoshi. The temperature-pressure-volume equation of state of platinum. *J. Appl. Phys.*, 105(1):13505, jan 2009. ISSN 0021–8979. doi:10.1063/1.3054331. URL <https://doi.org/10.1063/1.3054331>.
- [63] E. Menéndez-Proupin and A. K. Singh. Ab initio calculations of elastic properties of compressed Pt. *Phys. Rev. B*, 76(5):54117, aug 2007. doi:10.1103/PhysRevB.76.054117. URL <https://link.aps.org/doi/10.1103/PhysRevB.76.054117>.
- [64] F. D. Murnaghan. The Compressibility of Media under Extreme Pressures. *Proc. Natl. Acad. Sci.*, 30(9):244–247, sep 1944. ISSN 0027-8424. doi:10.1073/PNAS.30.9.244. URL <https://www.pnas.org/content/30/9/244>.
- [65] Y. Nanba, T. Ishimoto, and M. Koyama. Structural Stability of Ruthenium Nanoparticles: A Density Functional Theory Study. *J. Phys. Chem. C*, 121(49):27445–27452, dec 2017. ISSN 1932-7447. doi:10.1021/acs.jpcc.7b08672. URL <https://doi.org/10.1021/acs.jpcc.7b08672>.
- [66] B. Narayanan, A. Kinaci, F. G. Sen, M. J. Davis, S. K. Gray, M. K. Y. Chan, and S. K. R. S. Sankaranarayanan. Describing the Diverse Geometries of Gold from Nanoclusters to Bulk—A First-Principles-Based Hybrid Bond-Order Potential. *J. Phys. Chem. C*, 120(25):13787–13800, jun 2016. doi:10.1021/acs.jpcc.6b02934.
- [67] T. Nilsson Pingel, M. Jørgensen, A. B. Yankovich, H. Grönbeck, and E. Olsson. Influence of atomic site-specific strain on catalytic activity of supported nanoparticles. *Nat. Commun.*, 9(1):2722, 2018. ISSN 2041-1723. doi:10.1038/s41467-018-05055-1. URL <https://doi.org/10.1038/s41467-018-05055-1>.
- [68] P. P. Ylä-Mäihänen, J. Y. Y. Heng, F. Thielmann, and D. R. Williams. Inverse Gas Chromatographic Method for Measuring the Dispersive Surface Energy Distribution for Particulates. *Langmuir*, 24(17):9551–9557, aug 2008. doi:10.1021/la801676n.
- [69] J. Pal and T. Pal. Faceted metal and metal oxide nanoparticles: design, fabrication and catalysis. *Nanoscale*, 7(34):14159–14190, 2015. ISSN 2040-3364. doi:10.1039/C5NR03395K. URL <http://dx.doi.org/10.1039/C5NR03395K>.
- [70] N. Panagiotides and N. I. Papanicolaou. Diffusion of platinum adatoms and dimers on Pt(111) surface by molecular-dynamics simulation. *Int. J. Quantum Chem.*, 110(1):202–209, jan 2010. ISSN 0020-7608. doi:10.1002/qua.22045. URL <https://doi.org/10.1002/qua.22045>.
- [71] E. Panizon and R. Ferrando. Solid–solid transitions in Pd-Pt nanoalloys. *Phys. Rev. B*, 92(20):205417, nov 2015. doi:10.1103/PhysRevB.92.205417. URL <https://link.aps.org/doi/10.1103/PhysRevB.92.205417>.
- [72] N. I. Papanicolaou and N. Panagiotides. Interatomic potential for platinum and self-diffusion on pt(111) surface by molecular-dynamics simulation. In N. Russo, V. Y. Antonchenko, and E. S. Kryachko, editors, *SelfOrganization of Molecular Systems*, pages 335–344, Dordrecht, 2009. Springer Netherlands. ISBN 978-90-481-2590-6.
- [73] A. Parakh, S. Lee, K. A. Harkins, M. T. Kiani, D. Doan, M. Kunz, A. Doran, L. Hanson, S. Ryu, and X. W. Gu. Nucleation of Dislocations in 3.9 nm Nanocrystals at High Pressure. *Phys. Rev. Lett.*, 124(10):106104, mar 2020. doi:10.1103/PhysRevLett.124.106104. URL <https://link.aps.org/doi/10.1103/PhysRevLett.124.106104>.
- [74] A. Patra, J. E. Bates, J. Sun, and J. P. Perdew. Properties of real metallic surfaces: Effects of density functional semilocality and van der waals nonlocality. *Proceedings of the National Academy of Sciences*, 114(44):E9188–E9196, 2017. ISSN 0027-8424. doi:10.1073/pnas.1713320114. URL <https://www.pnas.org/content/114/44/E9188>.
- [75] S. Plimpton. Fast Parallel Algorithms for Short-Range Molecular Dynamics. *J. Comput. Phys.*, 117(1):1–19, 1995. ISSN 0021-9991. doi:<https://doi.org/10.1006/jcph.1995.1039>. URL <http://www.sciencedirect.com/science/article/pii/S002199918571039X>.
- [76] R. M. Rioux, H. Song, P. Yang, and G. A. Somorjai. Chapter 7 - platinum nanoclusters’ size and surface structure sensitivity of catalytic reactions. In B. Corain, G. Schmid, and N. Toshima, editors, *Met. Nanoclusters Catal. Mater. Sci.: Issue Size Control*, pages 149–166. Elsevier, Amsterdam, 2008. ISBN 978-0-444-53057-8. doi:<https://doi.org/10.1016/B978-044453057-8.50009-X>. URL <https://www.sciencedirect.com/science/article/pii/B978044453057850009X>.
- [77] A. Rodriguez, C. Amiens, B. Chaudret, M.-J. Casanove, P. Lecante, and J. S. Bradley. Synthesis and Isolation of Cuboctahedral and Icosahedral Platinum Nanoparticles. Ligand-Dependent Structures. *Chem. Mater.*, 8(8):1978–1986, aug 1996. doi:10.1021/cm960338l. URL <https://pubs.acs.org/sharingguidelines>.

- [78] B. Roldan Cuenya. Metal Nanoparticle Catalysts Beginning to Shape-up. *Acc. Chem. Res.*, 46(8):1682–1691, aug 2013. ISSN 0001-4842. doi:10.1021/ar300226p. URL <https://doi.org/10.1021/ar300226p>.
- [79] C. F. Sanz-Navarro, P.-O. Åstrand, D. Chen, M. Rønning, A. C. T. van Duin, T. Jacob, and W. A. Goddard. Molecular Dynamics Simulations of the Interactions between Platinum Clusters and Carbon Platelets. *J. Phys. Chem. A*, 112(7):1392–1402, feb 2008. ISSN 1089-5639. doi:10.1021/jp074806y. URL <https://pubs.acs.org/doi/10.1021/jp074806y>.
- [80] K. Scheerschmidt. *Empirical Molecular Dynamics: Possibilities, Requirements, and Limitations*, pages 213–244. Springer Berlin Heidelberg, Berlin, Heidelberg, 2007. ISBN 978-3-540-33401-9. doi:10.1007/11690320_10. URL https://doi.org/10.1007/11690320_10.
- [81] T.-R. Shan, B. D. Devine, T. W. Kemper, S. B. Sinnott, and S. R. Phillpot. Charge-optimized many-body potential for the hafnium/hafnium oxide system. *Phys. Rev. B*, 81(12):125328, mar 2010. doi:10.1103/PhysRevB.81.125328. URL <https://link.aps.org/doi/10.1103/PhysRevB.81.125328>.
- [82] G. Simmons. *Single Crystal Elastic Constants and Calculated Aggregate Properties*. J. Grad. Res. Cent. Southern Methodist University Press, 1965. URL <https://books.google.com/books?id=4q5esM1iatMC>.
- [83] U. K. Singh and M. Vannice. Kinetics of liquid-phase hydrogenation reactions over supported metal catalysts — a review. *Appl. Catal., A*, 213(1):1–24, 2001. ISSN 0926-860X. doi:[https://doi.org/10.1016/S0926-860X\(00\)00885-1](https://doi.org/10.1016/S0926-860X(00)00885-1). URL <http://www.sciencedirect.com/science/article/pii/S0926860X00008851>.
- [84] N. E. Singh-Miller and N. Marzari. Surface energies, work functions, and surface relaxations of low-index metallic surfaces from first principles. *Phys. Rev. B*, 80(23):235407, dec 2009. doi:10.1103/PhysRevB.80.235407. URL <https://link.aps.org/doi/10.1103/PhysRevB.80.235407>.
- [85] H. Song, F. Kim, S. Connor, G. A. Somorjai, and P. Yang. Pt Nanocrystals: Shape Control and Langmuir-Blodgett Monolayer Formation. *J. Phys. Chem. B*, 109(1):188–193, dec 2004. doi:10.1021/jp0464775.
- [86] M. O. Steinhauser and S. Hiermaier. A review of computational methods in materials science: Examples from shock-wave and polymer physics. *Int J Mol Sci*, 10(12):5135–5216, 2009. ISSN 1422-0067. doi:10.3390/ijms10125135. URL <https://www.mdpi.com/1422-0067/10/12/5135>.
- [87] A. J. Stephen, N. V. Rees, I. Mikheenko, and L. E. Macaskie. Platinum and palladium bio-synthesized nanoparticles as sustainable fuel cell catalysts. *Front. Energy Res.*, 7:66, 2019. ISSN 2296-598X. doi:10.3389/fenrg.2019.00066. URL <https://www.frontiersin.org/article/10.3389/fenrg.2019.00066>.
- [88] A. Stukowski. Visualization and analysis of atomistic simulation data with OVITO—the Open Visualization Tool. *Model. Simul. Mater. SC*, 18(1), JAN 2010. ISSN 0965-0393. doi:10.1088/0965-0393/18/1/015012.
- [89] T. Sun, K. Umemoto, Z. Wu, J.-C. Zheng, and R. M. Wentzcovitch. Lattice dynamics and thermal equation of state of platinum. *Phys. Rev. B*, 78(2):24304, jul 2008. doi:10.1103/PhysRevB.78.024304. URL <https://link.aps.org/doi/10.1103/PhysRevB.78.024304>.
- [90] E. B. Tadmor, R. S. Elliott, J. P. Sethna, R. E. Miller, and C. A. Becker. The potential of atomistic simulations and the knowledgebase of interatomic models. *JOM*, 63(7):17, 2011. ISSN 1543-1851. doi:10.1007/s11837-011-0102-6. URL <https://doi.org/10.1007/s11837-011-0102-6>.
- [91] J. Tersoff. New empirical approach for the structure and energy of covalent systems. *Phys. Rev. B*, 37(12):6991–7000, apr 1988. doi:10.1103/PhysRevB.37.6991. URL <https://link.aps.org/doi/10.1103/PhysRevB.37.6991>.
- [92] R. Tran, Z. Xu, B. Radhakrishnan, D. Winston, W. Sun, K. A. Persson, and S. P. Ong. Surface energies of elemental crystals. *Sci. Data*, 3(1):160080, 2016. ISSN 2052-4463. doi:10.1038/sdata.2016.80. URL <https://doi.org/10.1038/sdata.2016.80>.
- [93] W. R. Tyson and W. A. Miller. Surface free energies of solid metals: Estimation from liquid surface tension measurements. *Surf. Sci.*, 62(1):267–276, 1977. ISSN 0039-6028. doi:[https://doi.org/10.1016/0039-6028\(77\)90442-3](https://doi.org/10.1016/0039-6028(77)90442-3). URL <http://www.sciencedirect.com/science/article/pii/0039602877904423>.
- [94] L. Vega, J. Ruvireta, F. Viñes, and F. Illas. Jacob’s ladder as sketched by escher: Assessing the performance of broadly used density functionals on transition metal surface properties. *J. Chem. Theory Comput.*, 14(1):395–403, 2018. doi:10.1021/acs.jctc.7b01047. URL <https://doi.org/10.1021/acs.jctc.7b01047>. PMID: 29182868.
- [95] L. G. Verga and C.-K. Skylaris. Chapter 8 - dft modeling of metallic nanoparticles. In S. T. Bromley and S. M. Woodley, editors, *Computational Modelling of Nanoparticles*, volume 12 of *Frontiers of Nanoscience*, pages 239–293. Elsevier, 2018. doi:<https://doi.org/10.1016/B978-0-08-102232-0.00008-7>. URL <https://www.sciencedirect.com/science/article/pii/B9780081022320000087>.

- [96] S. H. Vosko, L. Wilk, and M. Nusair. Accurate spin-dependent electron liquid correlation energies for local spin density calculations: a critical analysis. *Can. J. Phys.*, 59:1200, aug 1980. ISSN 0008-4204. doi:10.1139/p80-159. URL <https://ui.adsabs.harvard.edu/abs/1980CaJPh...58.1200V>.
- [97] J. X. Wang, H. Inada, L. Wu, Y. Zhu, Y. Choi, P. Liu, W.-P. Zhou, and R. R. Adzic. Oxygen Reduction on Well-Defined Core-Shell Nanocatalysts: Particle Size, Facet, and Pt Shell Thickness Effects. *J. Am. Chem. Soc.*, 131(47):17298–17302, dec 2009. ISSN 0002-7863. doi:10.1021/ja9067645. URL <https://doi.org/10.1021/ja9067645>.
- [98] Y. Wang, B. Fugetsu, I. Sakata, C. Fujisue, S. Kabayama, N. Tahara, and S. Morisawa. Monolayered Platinum Nanoparticles as Efficient Electrocatalysts for the Mass Production of Electrolyzed Hydrogen Water. *Sci. Rep.*, 10(1):10126, 2020. ISSN 2045-2322. doi:10.1038/s41598-020-67107-1. URL <https://doi.org/10.1038/s41598-020-67107-1>.
- [99] C. Wei, Z. Zhao, A. Fisher, J. Zhu, and D. Cheng. Theoretical Study on the Structures and Thermal Properties of Ag-Pt-Ni Trimetallic Clusters. *J. Cluster Sci.*, 27(6):1849–1861, 2016. ISSN 1572-8862. doi:10.1007/s10876-016-1068-x. URL <https://doi.org/10.1007/s10876-016-1068-x>.
- [100] J. Wu, W. Gao, H. Yang, and J.-M. Zuo. Dissolution Kinetics of Oxidative Etching of Cubic and Icosahedral Platinum Nanoparticles Revealed by in Situ Liquid Transmission Electron Microscopy. *ACS Nano*, 11(2):1696–1703, feb 2017. doi:10.1021/acsnano.6b07541.
- [101] L. Xiao and L. Wang. Structures of Platinum Clusters: Planar or Spherical? *J. Phys. Chem. A*, 108(41):8605–8614, oct 2004. ISSN 1089-5639. doi:10.1021/jp0485035. URL <https://doi.org/10.1021/jp0485035>.
- [102] Y. Ye, V. Prakapenka, Y. Meng, and S.-H. Shim. Intercomparison of the gold, platinum, and MgO pressure scales up to 140 GPa and 2500 K. *J. Geophys. Res.: Solid Earth*, 122(5):3450–3464, may 2017. ISSN 2169-9313. doi:<https://doi.org/10.1002/2016JB013811>. URL <https://doi.org/10.1002/2016JB013811>.
- [103] M. Yokoo, N. Kawai, K. G. Nakamura, K.-i. Kondo, Y. Tange, and T. Tsuchiya. Ultrahigh-pressure scales for gold and platinum at pressures up to 550 GPa. *Phys. Rev. B*, 80(10), SEP 2009. ISSN 2469-9950. doi:10.1103/PhysRevB.80.104114.
- [104] K. Yun, Y.-H. Cho, P.-R. Cha, J. Lee, H.-S. Nam, J. S. Oh, J.-H. Choi, and S.-C. Lee. Monte Carlo simulations of the structure of Pt-based bimetallic nanoparticles. *Acta Mater.*, 60(12):4908–4916, 2012. ISSN 1359-6454. doi:<https://doi.org/10.1016/j.actamat.2012.05.032>. URL <http://www.sciencedirect.com/science/article/pii/S1359645412003527>.
- [105] W. Zang, G. Li, L. Wang, and X. Zhang. Catalytic hydrogenation by noble-metal nanocrystals with well-defined facets: a review. *Catal. Sci. Technol.*, 5(5):2532–2553, 2015. ISSN 2044-4753. doi:10.1039/C4CY01619J. URL <http://dx.doi.org/10.1039/C4CY01619J>.
- [106] C.-S. Zha, K. Mibe, W. A. Bassett, O. Tschauner, H.-K. Mao, and R. J. Hemley. P-v-t equation of state of platinum to 80gpa and 1900k from internal resistive heating/x-ray diffraction measurements. *J. Appl. Phys.*, 103(5):054908, 2008. doi:10.1063/1.2844358. URL <https://doi.org/10.1063/1.2844358>.
- [107] M. Zhou. A new look at the atomic level virial stress: on continuum-molecular system equivalence. *P Roy Soc Lond A Mat*, 459(2037):2347–2392, 2003. doi:10.1098/rspa.2003.1127. URL <https://royalsocietypublishing.org/doi/abs/10.1098/rspa.2003.1127>.
- [108] X. W. Zhou, R. A. Johnson, and H. N. G. Wadley. Misfit-energy-increasing dislocations in vapor-deposited CoFe/NiFe multilayers. *Phys. Rev. B*, 69(14):144113, apr 2004. doi:10.1103/PhysRevB.69.144113. URL <https://link.aps.org/doi/10.1103/PhysRevB.69.144113>.